

# Low Temperature 3D Printing of Drug Loaded Bioceramic Scaffolds and Implants



Susanne Meininger, Elke Vorndran, Miguel Castilho, Paulo Rui Fernandes and Uwe Gbureck

**Abstract** 3D powder printing (3DP) enables the fabrication of porous scaffolds with anisotropic aligned pores for bone tissue engineering and for the fabrication of custom made implants for cranio-maxillofacial surgery. By combining 3D printing and self-setting biocement matrices, a low temperature processing chain can be established for a simultaneous spatial control over both structure geometry and composition by using multi-colour printers. This contribution aims to highlight bioceramic material approaches in order to fabricate scaffolds and implants by 3DP with a special emphasis on the drug modification of such structures.

**Keywords** Bioceramics · 3D powder printing · Multi-colour printing · Bone implants · Drug delivery systems · Bone regeneration

## 1 Introduction

Additive manufacturing (AM) techniques are considered to be suitable methods to produce tissue replacement materials with a complex internal or external structure based on prefabricated structure designs or patient specific computer tomography data [1, 2]. The underlying principle of AM is a layerwise fabrication of near net shape structures by spatial control of material bonding with methods such as stereolithography [3], fused deposition modelling [4], 3D powder printing [5–10], 3D plotting [11, 12], melt electrospinning writing (MEW) [13, 14] or selective laser sintering [15]. Such generated structures may either directly serve as patient specific implants (PSI) or they can be used as porous scaffolds with aligned pores for

---

S. Meininger · E. Vorndran · U. Gbureck (✉)

Department of Functional Materials in Medicine and Dentistry, University of Würzburg, Würzburg, Germany

e-mail: [uwe.gbureck@fmz.uni-wuerzburg.de](mailto:uwe.gbureck@fmz.uni-wuerzburg.de)

M. Castilho

Department of Orthopedics, University Medical Center Utrecht, Utrecht, The Netherlands

P. R. Fernandes

IDMEC, Instituto Superior Técnico, Universidade de Lisboa, Lisbon, Portugal

© Springer Nature Switzerland AG 2019

P. R. Fernandes and P. J. da Silva Bartolo (eds.), *New Developments in Tissue Engineering and Regeneration*, Computational Methods in Applied Sciences 51,

[https://doi.org/10.1007/978-3-030-15372-4\\_4](https://doi.org/10.1007/978-3-030-15372-4_4)

guided tissue ingrowth. Materials processed by AM cover a broad range from pure metals [16], polymers [17], ceramics [18] or composites [19, 20], whereas every AM method requires specific material properties for processing.

A major application site for PSI prepared by AM are large sized bone defects predominantly in the cranio-maxillofacial area [21]. Bone is a highly hierarchical and slowly growing tissue with only a limited self-healing capacity, whereas in humans defects above a critical size of approximately 10 mm show no bony regeneration but the ingrowth of fibrous tissue [22]. Here, it is essential that the scaffold simulates natural bone tissue growth by providing adequate composition, morphology, structure, and mechanical properties. According to Karageorgiou et al. the main criteria for this purpose are sufficient mechanical strength within the range of cancellous bone as well as a highly interconnected porosity of at least 50% with pore sizes between 100 and 800  $\mu\text{m}$ , whereas pore characteristics (size, interconnectivity) are predominant parameters for nutrient exchange and cell ingrowth [23]. Since bone is a highly mineralized tissue with approx. 70 wt% hydroxyapatite as inorganic component, manufacturing approaches for bone scaffolds and implants usually comprise calcium phosphate compounds (e.g. hydroxyapatite, tricalcium phosphate, brushite) to mimic the bone ionic composition. Scaffold preparation either involves the fabrication of a green ceramic structure by the aid of polymeric binders, which are burnt out afterwards, or low temperature self-setting cement powder and pastes can be applied to avoid sintering and to produce hydrated calcium phosphate phases [6, 9, 17]. The latter is only possible by using non-thermal AM procedures (e.g. 3D plotting or printing), whereas the absence of heat enables the simultaneous deposition of drugs [24] or even living cells [25] within the scaffold.

This contribution aims to highlight material approaches to fabricate bioceramic scaffolds and implants by 3D printing with a special emphasis on the drug modification of such structures. The 3D powder printing technology enables the fabrication of porous scaffolds with anisotropically aligned pores in the sub millimeter range and has gained increasing attention for the fabrication of scaffolds for bone tissue engineering and custom made implants for cranio-maxillofacial surgery. Since 3D printing is a low temperature procedure it enables in addition a simultaneous spatial control over both structure geometry and composition by using multi-colour printers in conjunction with low temperature self-setting ceramic matrices.

## 2 3D Printing Technology

3D powder printing (3DP) is an attractive technology due to its rapid and inexpensive model making ability in technical or medical applications, e.g. for the fabrication of casting moulds [26] or biodegradable and osteoactive implants [10, 27–31]. The 3D powder printing technique forms a 3-dimensional structure based on thin powder layers and a binding agent, which is locally sprayed onto the powder leading to a localised solidification of the powder particles [32, 33]. The solidification process can be either induced by a physical mechanism (e.g. organic liquid, swelling or partial

dissolution of polymeric additives, phase changes) or by a chemical reaction (e.g. hydraulic cement setting, acid-base reaction). A detailed description of the different hardening possibilities during 3DP can be found in literature [34]. Although the reactive binding component is often distributed in the powder and the printing liquid only starts the binding process, the printing liquid will be denominated as “binder” within this article.

The general underlying principle of 3DP is demonstrated in Fig. 1a. In a first step, a thin and smooth layer of powder is prepared in the building chamber by a counter-clockwise rotating roller transferring powder from the reservoir to the printing bed in a defined layer thickness. Secondly, the print head locally sprays the binder on the powder surface such that the first layer of the implant structure is printed surrounded by unreacted powder. After this the roller moves back, the powder reservoir lifts up by the thickness of one layer and the roller moves another powder layer to the printing bed which is at the same time lowered by one layer thickness. The second printed layer of the structure is created on top of the first one and both layers stick together by binder diffusion due to capillary forces of the powder bed. This process repeats until all of the layers of the sample are printed. The samples are then removed from the printing bed and cleaned from residual unreacted powder. Cleaning is commonly performed by blowing air, whereas the surface finish of the printed part can be improved by vibration with the addition of smaller particles. While cleaning of the outer surface is relatively easy, the removal of loose powder particles from the inner part (e.g. small pores <500  $\mu\text{m}$  intended for blood vessel ingrowth) is much more demanding and may require additionally wet methods such as ultrasonication or microwave assisted boiling of the sample [35]. However, these procedures are only possible in liquids which do not dissolve the binder to avoid mechanical disintegration of the printed sample. An approach for an improved depowdering of porous implants suggested by Butscher et al. [36] is based on the design of an outer cage with windows, which are large enough to enable depowdering, but at the same time can trap loosely bound (3D printed) filler particles in the inside of the implant. Since the initial strength of the printed parts is in most cases relatively low, a post-processing regime is commonly applied to increase strength, e.g. by polymer infiltration [37], repeated immersion in binder liquid for hydraulic setting systems [9] or sintering [38]. Generally, it has to be taken into account that the 3DP process is an anisotropic manufacturing process due to the layer wise preparation of thin powder layers by a roller. This means that the final size of the printed structure may also show an anisotropic deviation from the theoretical values and this also applies for other properties such as the mechanical strength [39, 40].

Commercially available 3D powder printing systems (e.g. Z-Corp systems) commonly use thermally working drop-on-demand print-heads (Fig. 1b, c), in which the binder droplets (approx. 30 picoliter in volume [41]) are created in thin nozzles and ejected by a steam bubble formed by thermal evaporation of the binder liquid. Such thermal print heads are comparatively cheap, but problems may occur if either the binding liquid dries within the nozzles or solids are precipitated during binder evaporation, both leading to a clogging of the nozzles and hence a reduction of print head life time and printing quality. An alternative is the use of piezoelectric print

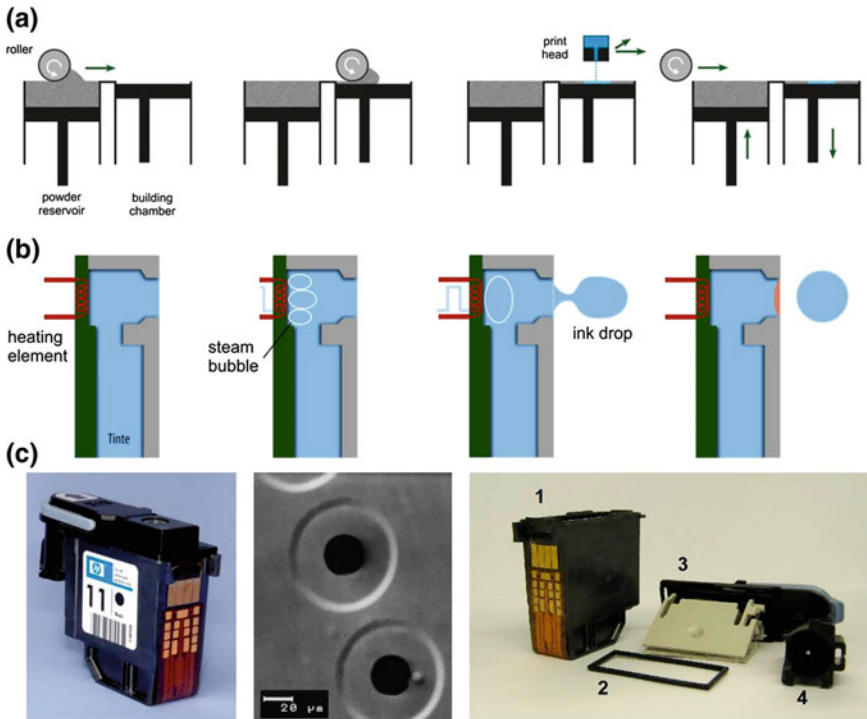


**Fig. 1** **a** Fabrication steps for additive manufacturing of a sample by 3D printing. 1–2: a roller transfers a thin powder layer to the building room, 3: localised application of binder liquid leads to spatially controlled hardening of the powder. 4: repetition of 1–3 results in the fusion of the printed layers and the formation of a three dimensional object. **b** Thermally working print-head, which ejects droplets through a nozzle by binder evaporation. **c** Left: commercially available print-head (used in ZCorp Printers), middle: SEM of print-head nozzles, right: single parts of the print-head

heads, which form the binder drops by the sudden volume change of a piezoelectric material, which causes an acoustic pulse and hence forms an ink-droplet in the nozzle [42].

Printing systems are nowadays available from various companies enabling the fabrication of samples spanning from the millimeter to the meter range [43]. Worth to note is, that all commercial 3D powder printers (including materials) up to now are designed for civil engineering purpose, their use in biomedical engineering is sometimes difficult due to the special requirements (e.g. cleaning, sterilization etc.) of this field. Similar, most of the commercially available print heads for 3DP systems stem from ordinary ink jet printers and are hence filled with ink, which has to be carefully removed prior to use. Even small ink residues within the print head may also lead to clogging of the nozzles when using experimental binder liquids, in addition any ink contamination of the fabricated samples may have a detrimental effect on the biocompatibility.

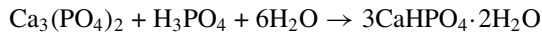
### 3 Material Approaches to 3D Powder Printing of Ceramic Bone Scaffolds

3D powder printed samples are characterized by a high microporosity >30 vol.%, which is a result from the voids between the loosely packed powder particles during the fabrication process. This microporosity is beneficial since it enables nutrients diffusion to support cell ingrowth and vascularization into larger sized macropores with sizes of a few 100  $\mu\text{m}$  [20, 44]. Many recent studies have dealt with the adaptation of the 3D printing process to the fabrication of bone substitutes from calcium phosphate based powders such as hydroxyapatite (HA) [45, 46],  $\beta$ -tricalcium phosphate ( $\beta$ -TCP) [47, 48], biphasic HA/ $\beta$ -TCP mixtures (BCP) [49, 50],  $\beta$ -TCP/calcium pyrophosphate ceramics [51], calcium polyphosphates [52] or brushite [9]. Most of the investigated material systems require a final sintering step for binder burn out and densification of the ceramic. This usually results in the formation of a microcrystalline texture and—in case of hydroxyapatite—practically insoluble implants. Direct printing of more soluble nanocrystalline hydroxyapatite (HA) similar to the mineral phase of bone (e.g. by a cement setting reaction to avoid sintering) is difficult and would require the use of polymeric additives to control liquid binder localisation over a long time period. The reason for this is the low crystal growth rate of HA leading to a low reactivity between solid and liquid during printing. Preferably, 3D printing of nanoscale HA samples is performed in a two-step regime, in which first the sample is fabricated using a fast setting reaction (e.g. brushite formation or use of calcium sulphate powders), followed by a hydrothermal treatment of the finished part to transform it into HA without change of size and shape [8, 27, 30].

A general requirement for powders used for 3D printing is a sufficient flowability to form thin powder layers with a smooth surface to obtain high printing quality. This property is associated with the particle size distribution of the powder. It has been demonstrated that ideal particle sizes for 3D powder printing are in the range of 15–35  $\mu\text{m}$  [7, 53, 54]. Larger particles in the size range of the individual powder layer thickness (80–150  $\mu\text{m}$ ) may interfere with printing quality similar to small particle fractions <5  $\mu\text{m}$ , which build up large sized agglomerates in the millimeter range. An approach to improve the powder flowability and hence the quality of the powder surface is based on a plasma coating of the particles with  $\text{SiO}_x$  nanoparticles as demonstrated by Butscher et al. [7]. These nanoparticles act as spacer between the larger size powder particles and hence reduce attractive van der Waals forces. The printing quality can also be increased by a controlled humidification of the powder surface prior to printing. This is thought to stabilize the loosely packed particles to avoid movement of the particle layer (and hence the printed sample) during recoating with the next powder layer. Indeed, it was demonstrated that for a low layer thickness of 44  $\mu\text{m}$ , applied moisture had a strong positive effect on geometrical sample accuracy, especially when only a small number of samples was simultaneously printed [5].

Since the binder liquid is sprayed onto a porous powder bed, also a rapid hardening reaction is necessary to reduce uncontrolled binder spreading due to capillary

forces and to ensure high printing quality. Such hardening reactions can be based on different mechanisms as described above, whereas cement setting reaction offer the advantage of a low temperature processing regime to produce hydrated ceramics (e.g. brushite) and to simultaneously deposit organic drugs within the printed matrix. Suitable bioceramics are based on reactive calcium phosphate powders (e.g. TTCP or  $\alpha$ -TCP), which react during printing with acidic phosphate solutions to form a matrix of secondary calcium phosphates in a fast dissolution—precipitation reaction:



The high reactivity leads to a rapid setting and solidification within seconds and mostly prevents undesired binder spreading such that macropores down to a size of approx. 300–400  $\mu\text{m}$  can be printed within a structure (Fig. 2). Since the degree of conversion during printing is small, commonly a post-hardening regime by short immersion cycles in binder liquid are applied to increase both the amount of brushite formed in the sample as well as the mechanical performance. Following this, compressive strength of up to 22 MPa can be obtained [9]. An alternative setting reaction was recently described by Mandal et al. [55], who used diluted phytic acid solution as binder liquid, which formed calcium chelates with tetracalcium phosphate powder during 3D printing. This approach was beneficial since the printed structured did not convert into low soluble hydroxyapatite during prolonged immersion in physiological solution. The strength of 3D printed samples can be generally increased by polymer impregnation, which can be either performed during the printing process or post printing [56].

3D printed calcium phosphate structures were demonstrated to have an excellent biocompatibility both under in vitro [53, 57] and in vivo conditions [20, 58–61]. Klammert et al. could prove the biocompatibility of printed brushite/monetite scaffolds in an osteoblastic cell culture model [57] with an application in bone replacement by printing highly accurate craniofacial implants [21]. The biocompatibility and osteoconductivity of such printed implants was confirmed in vivo by Habibovic et al. after implantation in bone in a sheep model [58]. Surprisingly, the same authors were also able to demonstrate that the materials were at the same time osteoinductive leading to the formation of bone after intramuscular implantation. Cell-biological aspects of 3D printed implant resorption were investigated by Detsch et al. [53] by seeding the macrophage cell line RAW 264.7 on 3D printed HA,  $\beta$ -TCP and BCP surfaces. All such materials promoted the differentiation of macrophage precursor cells into bone-resorbing osteoclast-like cells, whereas a 60:40 mixture of HA and  $\beta$ -TCP showed the most promising results regarding cell growth, differentiation and hence material degradation. The latter can also be adjusted by post-processing of 3D printed samples, e.g. by autoclaving brushite to form monetite ( $\text{CaHPO}_4$ ). Monetite ceramics show an enhanced in vivo degradation profile [9, 62], likely because of the absence of a phase transformation into a lower soluble HA phase in vivo. A veterinary application of 3D printed brushite samples was investigated by Castilho et al. [63], who fabricated a customized calcium phosphate implant (composed of

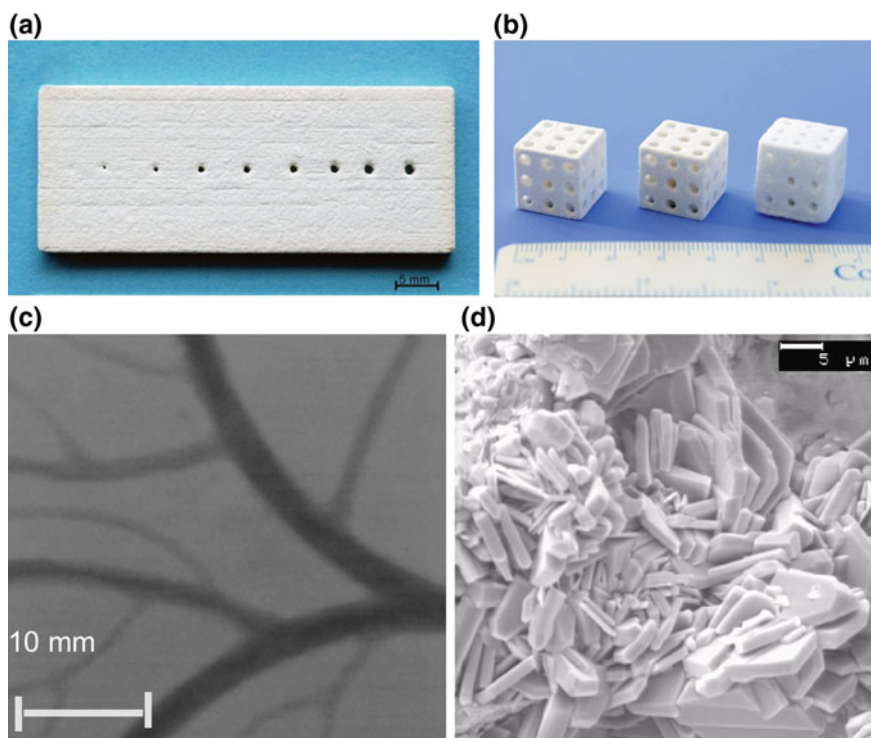


**Fig. 2** **a, b** Examples of 3D printed macroporous brushite samples, **c** X-ray micrograph of a branched pore system in a sample and **d** microstructure of the samples after  $3 \times 30$  s post hardening in 20% phosphoric acid

brushite, monetite and tricalcium phosphate) for canine cruciate ligament treatment by tibial tuberosity advancement in dogs (Fig. 3).

The implant was designed using a suitable topology optimization methodology in order to maximize permeability due to an overall porosity of 59.2%. The latter was achieved by the combination of process-immanent microporosity of approximately 40% and a designed interconnected macroporous network with pore sizes of  $845 \mu\text{m}$ . The mechanical properties of such printed implants were in the range of trabecular bone enabling complete restoration of the dog's limb function without any adverse complications.

## 4 Drug Modification of 3D Printed Implants

Drug delivery systems (DDS) are designed for the controlled release of bioactives directly into a defined target tissue and to maintain a sufficient therapeutic level of the drug over a defined period of time. This should avoid risks of a systemic

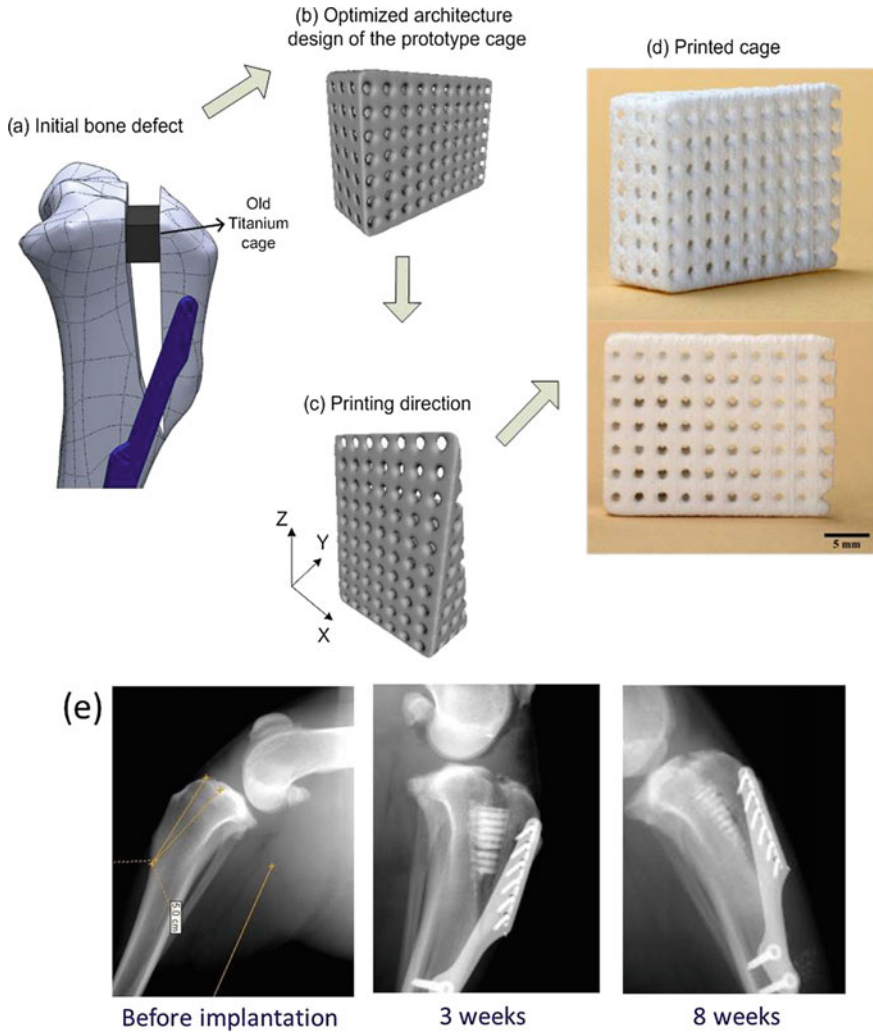


**Fig. 3** a–d Fabrication regime of a calcium phosphate cage resulting from the periodic repetition of an optimized unit cell with  $1000\ \mu\text{m}$  macropore size; e X-ray micrographs of the implanted cage in the dog left stifle joint after different time intervals post operatively. Unpublished images from Ref. [63]



drug application, especially side effects due to a high plasma concentration, a low bioavailability resulting from low blood supply or biological barriers of target tissue, or an elimination or inactivation of the drug during in vivo transport [64]. Common modifications in the area of bone tissue regeneration include bioactives to induce angiogenesis or osteogenesis [65], chemotherapeutical agents to treat cancer [66] or antibiotics for infection treatment or prophylaxis [67]. Recent developments concern the use of microporous 3D printed CaP-scaffolds as drug carriers. Drug modification is possible by immersion of the porous ceramic scaffolds in an aqueous drug solution leading to a homogeneous distribution of the drug within the scaffold structure [68–70]. The adsorption behaviour and the release kinetic of antibiotics on different printed calcium phosphate matrices (brushite, monetite, hydroxyapatite) are predominantly determined by physical properties like porosity and specific surface area of the matrices or drug-matrix interactions [68]. Commonly, a quantitative release within 2 days was observed due to the microporosity with pore sizes in the range of 10–15  $\mu\text{m}$ . A sustained release was achieved by infiltration of the DDS with a degradable polymer [68]. Later, an in vivo study showed, that simultaneous manual application of BMP-2 within a 3D printed biphasic calcium phosphate scaffold enhance bone growth compared to unloaded or to scaffolds with a delayed BMP application [70, 71].

A more sophisticated approach to create DDS by additive manufacturing is the use of multiphase-printers [72], which enable the simultaneous processing of different materials in one scaffold. An example are multicolour-3D printers, in which the colour information can be used to deposit bioactive compounds at desired locations in the 3D scaffolds for a spatial control of drug release kinetics and tissue response. For this process, drugs will be dissolved or dispersed in a solution and printed within defined areas of the scaffold, whereas the solutions have to be adjusted to gain optimal printability [73]. This was firstly demonstrated by Wu et al. [74], who controlled the release rate of dyes (methylene blue and alizarin yellow) as model drug from polymers (polycaprolactone, polyethylene oxide) by adjusting the local drug concentration and matrix composition. The authors demonstrated that 3D printing is not limited to adjust only zero order release kinetics but can also produce multiple diffusion gradients within a single device to create more complicated drug release profiles not easily achieved with conventional processing techniques [68]. Following studies dealt with the fabrication of polymeric DDS with controlled release patterns of single or multiple drugs [75, 76], e.g. by printing multilayer concentric cylinders, in which each layer can be loaded with a specific drug to obtain an orderly release profile from the outside to the center of the DDS with peak concentrations at 8–12 days intervals. Bone tuberculosis treatment by loading the printed DDS with either isoniazid or rifampicin was discussed to be an application [76]. Another study by Yu et al. investigated the release behaviour of acetaminophen from depot loaded ethylcellulose tablets. Release-retarding material gradients and drug-free diffusion barriers were utilized to gain a constant release rate over a period of 5–13 h governed by matrix erosion and diffusion process [75].

An application of this concept to ceramic bone implants used a commercially available multi-colour printer for sample preparation [24], in which the black chan-

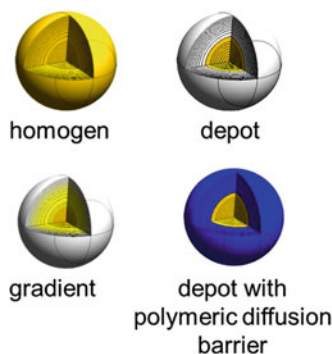
nel was used for applying the binder, while the other three channels were filled with solutions containing either BMP-2, vancomycin, heparin as drugs or a chitosan solution to produce either homogeneous, depot or gradient drug loadings (Fig. 4a). A spatial resolution of approximately 300  $\mu\text{m}$  of the drugs within the matrix was achieved by using a cellulose modified tricalcium phosphate powder. Drug release kinetics were shown to depend on the drug localisation within the scaffolds; while homogeneously loaded scaffolds provided first order release kinetics, drug depots or gradients resulted in zero order release over a period of 3–4 days with release rates in the range 0.68–0.96%/h (Fig. 4b).

A crucial prerequisite for such 3D printed DDS is that the pharmacological activity of imprinted drugs is maintained until final release. This is somewhere challenging since the fabrication regime includes harsh conditions, e.g. (1) parts of the binder solution are thermally evaporated during printing, (2) high shear forces occur during bubble ejection or (3) the acid pH during setting of the above mentioned brushite cement matrix. While (1) and (2) seemed to have only a minor effect on drug activity (demonstrated by purging the solutions through the print-heads without cement matrix), (3) seemed to be a parameter diminishing the activity of delicate protein based factors. Indeed, only for pH insensitive drugs like vancomycin it was possible to demonstrate more or less unchanged activity after the whole process chain and release from the brushite matrix (Fig. 5a). A solution to this problem might be the use of neutral setting cements for 3D printing based on the formation of struvite ( $\text{MgNH}_4\text{PO}_4 \cdot 6\text{H}_2\text{O}$ ) from magnesium phosphate powder and ammonium phosphate solution. Indeed, by using this approach it was possible to measure a certain BMP-2 activity after printing and release, however the determined activities were quite low compared to the activity of the used binder solution (Fig. 5b) [77]. This is thought to be a result of the quite low porosity of struvite cements (5–7% according to [78]), which may have led to a physical entrapment of the drug within the matrix.

## 5 Conclusion

3D powder printing of ceramic implants and scaffolds enables the fabrication of patient specific implants or macroporous scaffolds from a broad range of materials. The possibility to perform the process at room temperature by using self-setting ceramic bone cements offers the possibility for a simultaneous control over geometry, porosity and composition. Such cements are hydrated phases of calcium or magnesium phosphates (brushite, monetite, struvite) with an enhanced degradation ability compared to traditionally used sintered materials such as hydroxyapatite or tricalcium phosphate. The progress in developing low temperature rapid prototyping systems using a cement setting reaction may open the possibility to fabricate scaffolds of different compositions (ceramic, hydrogel) which are simultaneously loaded with bioactives to control release profile and cellular response. Clearly, such a fabrication chain of drug loaded samples would require a processing under sterile conditions since common sterilisation procedures (heat,  $\gamma$ -irradiation) may negatively affect the

**(a) Release study**



binder application [%]				colour code
Cyan (print-head 3)	Magenta (print-head 2)	Yellow (print-head 1)	White (print-head 0)	
bioactive 3	bioactive 2	bioactive 1	binder 100	white
-	-	-	15	yellow
-	18	-	82	magenta
11	-	-	89	cyan
34	12	-	54	blue
-	31	53	16	red
8	-	23	69	green
33	35	31	1	black

**(b)**

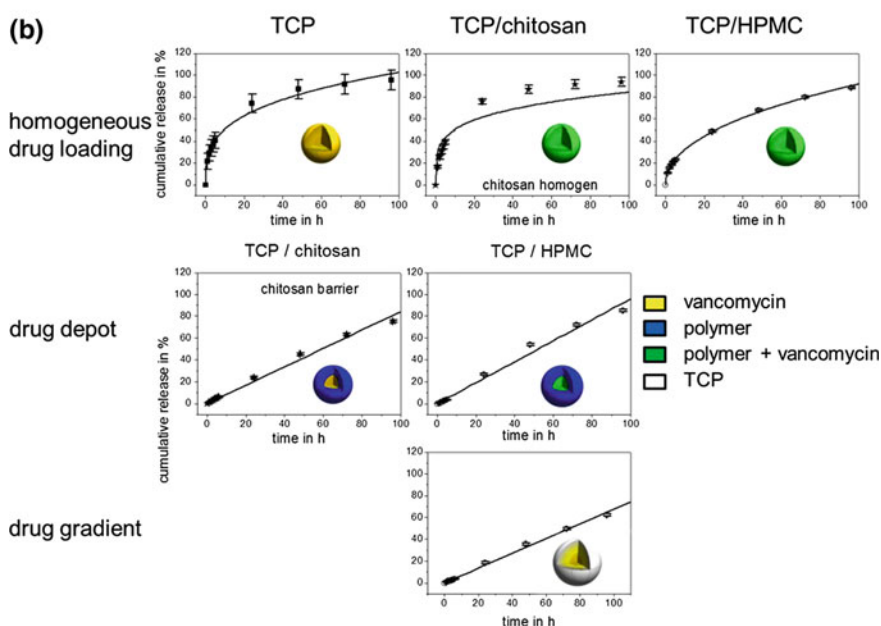


**Fig. 4** a Spherical bioceramic samples prepared by 3D powder printing with either homogeneous, depot or graded drug loading. Hardening of samples is achieved by printing binder solution ( $H_3PO_4$ ) with the black print-head, while localized deposition of drugs is achieved by additional print-heads based on the colour information of each sample. b Vancomycin release kinetics from brushite samples in PBS buffer over a course of 4 days [24]. The ceramic spheres were printed with TCP powder, partially mixed with hydroxymethyl propyl cellulose (HPMC), and phosphoric acid as binder. The vancomycin or chitosan was locally incorporated within the samples by spraying of the antibiotic or chitosan solution through a print head (Color figure online)

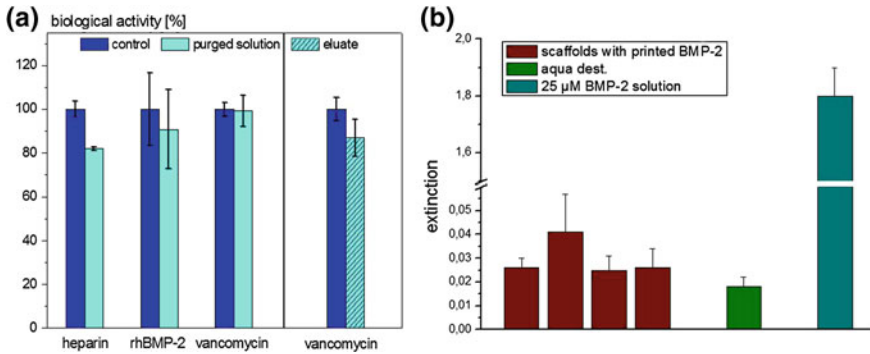


**Fig. 5** **a** Pharmaceutical activity of drugs after applying through the print-head and after the whole process chain; matrix: brushite from TCP powder and phosphoric acid as binder [24]; **b** BMP-2 activity after release from a neutral pH setting struvite matrix [77] (Color figure online)

pharmacological activity of many imprinted drugs. Engineering suitable and reliable printers for sterile processing is likely the next step in the fabrication and clinical application of drug or cell loaded ceramic implants.

**Acknowledgements** Paulo Rui Fernandes would like to thank to Fundação para a Ciência e Tecnologia (Portugal) for the support through project PTDC/BBB-BMC/5655/2014 and LAETA project UID/EMS/50022/2019.

## References

1. Vorndran E, Moseke C, Gbureck U (2015) 3D printing of ceramic implants. *MRS Bull* 40:127–136
2. Garrett B (2014) 3D printing: new economic paradigms and strategic shifts. *Glob Policy* 5:70–75
3. Melchels FPW, Feijen J, Grijpma DW (2010) A review on stereolithography and its applications in biomedical engineering. *Biomaterials* 31:6121–6130
4. Teo EY, Ong SY, Chong MSK, Zhang ZY, Lu J, Mochhala S et al (2011) Polycaprolactone-based fused deposition modeled mesh for delivery of antibacterial agents to infected wounds. *Biomaterials* 32:279–287
5. Butscher A, Bohner M, Doebelin N, Galea L, Loeffel O, Muller R (2013) Moisture based three-dimensional printing of calcium phosphate structures for scaffold engineering. *Acta Biomater* 9:5369–5378
6. Butscher A, Bohner M, Hofmann S, Gauckler L, Muller R (2011) Structural and material approaches to bone tissue engineering in powder-based three-dimensional printing. *Acta Biomater* 7:907–920
7. Butscher A, Bohner M, Roth C, Ernstberger A, Heuberger R, Doebelin N et al (2012) Printability of calcium phosphate powders for three-dimensional printing of tissue engineering scaffolds. *Acta Biomater* 8:373–385
8. Suwanprateeb J, Suvannapruk W, Wasoontararat K (2010) Low temperature preparation of calcium phosphate structure via phosphorization of 3D-printed calcium sulfate hemihydrate based material. *J Mater Sci Mater Med* 21:419–429

9. Gbureck U, Hozel T, Klammert U, Wurzler K, Muller FA, Barralet JE (2007) Resorbable dicalcium phosphate bone substitutes prepared by 3D powder printing. *Adv Func Mater* 17:3940–3945
10. Leukers B, Gulkan H, Irsen SH, Milz S, Tille C, Schieker M et al (2005) Hydroxyapatite scaffolds for bone tissue engineering made by 3D printing. *J Mater Sci Mater Med* 16:1121–1124
11. Luo YX, Lode A, Akkineni AR, Gelinsky M (2015) Concentrated gelatin/alginate composites for fabrication of pre-designed scaffolds with a favorable cell response by 3D plotting. *RSC Adv* 5:43480–43488
12. Luo YX, Lode A, Sonntag F, Nies B, Gelinsky M (2013) Well-ordered biphasic calcium phosphate-alginate scaffolds fabricated by multi-channel 3D plotting under mild conditions. *J Mater Chem B* 1:4088–4098
13. Brown TD, Edin F, Detta N, Skelton AD, Huttmacher DW, Dalton PD (2014) Melt electrospinning of poly( $\epsilon$ -caprolactone) scaffolds: phenomenological observations associated with collection and direct writing. *Mater Sci Eng C Mater Biol Appl* 45:698–708
14. Mota C, Puppi D, Gazzarri M, Bartolo P, Chiellini F (2013) Melt electrospinning writing of three-dimensional star poly( $\epsilon$ -caprolactone) scaffolds. *Polym Int* 62:893–900
15. Sadeghian Z, Heinrich JG, Moztaradeh F (2004) Direct laser sintering of hydroxyapatite implants by layer-wise slurry deposition (LSD). *CFI-Ceramic Forum Int* 81:E39–E43
16. Ryan GE, Pandit AS, Apatsidis DP (2008) Porous titanium scaffolds fabricated using a rapid prototyping and powder metallurgy technique. *Biomaterials* 29:3625–3635
17. Huttmacher DW (2001) Scaffold design and fabrication technologies for engineering tissues—state of the art and future perspectives. *J Biomater Sci Polym Ed* 12:107–124
18. Legeros RZ, Lin S, Rohanizadeh R, Mijares D, Legeros JP (2003) Biphasic calcium phosphate bioceramics: preparation, properties and applications. *J Mater Sci Mater Med* 14:201–209
19. Bakarich SE, Gorkin R, Panhuis MIH, Spinks GM (2014) Three-dimensional printing fiber reinforced hydrogel composites. *ACS Appl Mater Interfaces* 6:15998–16006
20. Inzana JA, Olvera D, Fuller SM, Kelly JP, Graeve OA, Schwarz EM et al (2014) 3D printing of composite calcium phosphate and collagen scaffolds for bone regeneration. *Biomaterials* 35:4026–4034
21. Klammert U, Gbureck U, Vorndran E, Rodiger J, Meyer-Marcotty P, Kubler AC (2010) 3D powder printed calcium phosphate implants for reconstruction of cranial and maxillofacial defects. *J Cranio Maxillofac Surg* 38:565–570
22. Aaboe M, Pinholt EM, Hjortinghansen E (1995) Healing of experimentally created defects—a review. *Br J Oral Maxillofac Surg* 33:312–318
23. Karageorgiou V, Kaplan D (2005) Porosity of 3D biomaterial scaffolds and osteogenesis. *Biomaterials* 26:5474–5491
24. Vorndran E, Klammert U, Ewald A, Barralet JE, Gbureck U (2010) Simultaneous immobilization of bioactives during 3D powder printing of bioceramic drug-release matrices. *Adv Func Mater* 20:1585–1591
25. Lode A, Krujatz F, Bruggemeier S, Quade M, Schutz K, Knaack S et al (2015) Green bio-printing: fabrication of photosynthetic algae-laden hydrogel scaffolds for biotechnological and medical applications. *Eng Life Sci* 15:177–183
26. Vorndran E, Wunder K, Moseke C, Biermann I, Muller FA, Zorn K et al (2011) Hydraulic setting  $Mg_3(PO_4)_2$  powders for 3D printing technology. *Adv Appl Ceram* 110:476–481
27. Seitz H, Rieder W, Irsen S, Leukers B, Tille C (2005) Three-dimensional printing of porous ceramic scaffolds for bone tissue engineering. *J Biomed Mater Res Part B Appl Biomater* 74B:782–788
28. Leukers B, Gulkan H, Irsen SH, Milz S, Tille C, Seitz H et al (2005) Biocompatibility of ceramic scaffolds for bone replacement made by 3D printing. *Materialwiss Werkstofftech* 36:781–787
29. Gbureck U, Holzel T, Doillon CJ, Muller FA, Barralet JE (2007) Direct printing of bioceramic implants with spatially localized angiogenic factors. *Adv Mater* 19:795–+
30. Gbureck U, Holzel T, Thull R, Muller FA, Barralet JE (2006) Preparation of nanocrystalline hydroxyapatite scaffolds by 3D powder printing. *Cytotherapy* 8:14

31. Bergmann C, Lindner M, Zhang W, Koczur K, Kirsten A, Telle R et al (2010) 3D printing of bone substitute implants using calcium phosphate and bioactive glasses. *J Eur Ceram Soc* 30:2563–2567
32. Bose S, Vahabzadeh S, Bandyopadhyay A (2013) Bone tissue engineering using 3D printing. *Mater Today* 16:496–504
33. Hwa LC, Rajoo S, Noor AM, Ahmad N, Uday MB (2017) Recent advances in 3D printing of porous ceramics: a review. *Curr Opin Solid State Mater Sci* 21:323–347
34. Kumar A, Mandal S, Barui S, Vasireddi R, Gbureck U, Gelinsky M et al (2016) Low temperature additive manufacturing of three dimensional scaffolds for bone-tissue engineering applications: processing related challenges and property assessment. *Mater Sci Eng R Rep* 103:III-39
35. Sachs EM CM, Bredt JF (1996) Process for removing loose powder particles from interior passages of a body. United States: U.S. Patent and Trademark Office. Massachusetts Institute of Technology, pp 5, 490, 882
36. Butscher A, Bohner M, Doebelin N, Hofmann S, Muller R (2013) New depowdering-friendly designs for three-dimensional printing of calcium phosphate bone substitutes. *Acta Biomater* 9:9149–9158
37. Suwanprateeb J, Sanngam R, Suwanpreuk W (2008) Fabrication of bioactive hydroxyapatite/bis-GMA based composite via three dimensional printing. *J Mater Sci Mater Med* 19:2637–2645
38. Winkel A, Meszaros R, Reinsch S, Muller R, Travitzky N, Fey T et al (2012) Sintering of 3D-printed glass/HAp composites. *J Am Ceram Soc* 95:3387–3393
39. Castilho M, Dias M, Gbureck U, Groll J, Fernandes P, Pires I et al (2013) Fabrication of computationally designed scaffolds by low temperature 3D printing. *Biofabrication* 5
40. Meininger S, Mandal S, Kumar A, Groll J, Basu B, Gbureck U (2016) Strength reliability and in vitro degradation of three-dimensional powder printed strontium-substituted magnesium phosphate scaffolds. *Acta Biomater* 31:401–411
41. Creagh LT, McDonald M (2003) Design and performance of inkjet print heads for non-graphic-arts applications. *MRS Bull* 28:807–811
42. de Gans BJ, Duineveld PC, Schubert US (2004) Inkjet printing of polymers: state of the art and future developments. *Adv Mater* 16:203–213
43. Lu K, Reynolds WT (2008) 3DP process for fine mesh structure printing. *Powder Technol* 187:11–18
44. Boyan BD, Hummert TW, Dean DD, Schwartz Z (1996) Role of material surfaces in regulating bone and cartilage cell response. *Biomaterials* 17:137–146
45. Will J, Melcher R, Treul C, Travitzky N, Kneser U, Polykandriotis E et al (2008) Porous ceramic bone scaffolds for vascularized bone tissue regeneration. *J Mater Sci Mater Med* 19:2781–2790
46. Suwanprateeb J, Sanngam R, Panyathanmaporn T (2010) Influence of raw powder preparation routes on properties of hydroxyapatite fabricated by 3D printing technique. *Mater Sci Eng C Mater Biol Appl* 30:610–617
47. Fielding GA, Bandyopadhyay A, Bose S (2012) Effects of silica and zinc oxide doping on mechanical and biological properties of 3D printed tricalcium phosphate tissue engineering scaffolds. *Dent Mater* 28:113–122
48. Vorndran E, Klarner M, Klammert U, Grover LM, Patel S, Barralet JE et al (2008) 3D powder printing of beta-tricalcium phosphate ceramics using different strategies. *Adv Eng Mater* 10:B67–B71
49. Castilho M, Moseke C, Ewald A, Gbureck U, Groll J, Pires I et al (2014) Direct 3D powder printing of biphasic calcium phosphate scaffolds for substitution of complex bone defects. *Biofabrication* 6
50. Seitz H, Deisinger U, Leukers B, Detsch R, Ziegler G (2009) Different calcium phosphate granules for 3-D printing of bone tissue engineering scaffolds. *Adv Eng Mater* 11:B41–B46
51. Gbureck U, Hoelzel T, Biermann I, Barralet JE, Grover LM (2008) Preparation of tricalcium phosphate/calcium pyrophosphate structures via rapid prototyping. *J Mater Sci Mater Med* 19:1559–1563

52. Shanjani Y, De Croos JNA, Pilliar RM, Kandel RA, Toyserkani E (2010) Solid freeform fabrication and characterization of porous calcium polyphosphate structures for tissue engineering purposes. *J Biomed Mater Res Part B Appl Biomater* 93B:510–519
53. Detsch R, Schaefer S, Deisinger U, Ziegler G, Seitz H, Leukers B (2011) In vitro-osteoclastic activity studies on surfaces of 3D printed calcium phosphate scaffolds. *J Biomater Appl* 26:359–380
54. Tay BY, Evans JRG, Edirisinghe MJ (2003) Solid freeform fabrication of ceramics. *Int Mater Rev* 48:341–370
55. Mandal S, Meininger S, Gbureck U, Basu B (2018) 3D powder printed tetracalcium phosphate scaffold with phytic acid binder: fabrication, microstructure and in situ X-ray tomography analysis of compressive failure. *J Mater Sci Mater Med* 29
56. Vella JB, Trombetta RP, Hoffman MD, Inzana J, Awad H, Benoit DSW (2018) Three dimensional printed calcium phosphate and poly(caprolactone) composites with improved mechanical properties and preserved microstructure. *J Biomed Mater Res Part A* 106:663–672
57. Klammert U, Reuther T, Jahn C, Kraski B, Kubler AC, Gbureck U (2009) Cytocompatibility of brushite and monetite cell culture scaffolds made by three-dimensional powder printing. *Acta Biomater* 5:727–734
58. Habibovic P, Gbureck U, Doillon CJ, Bassett DC, van Blitterswijk CA, Barralet JE (2008) Osteoconduction and osteoinduction of low-temperature 3D printed bioceramic implants. *Bio-materials* 29:944–953
59. Fielding G, Bose S (2013) SiO<sub>2</sub> and ZnO dopants in three-dimensionally printed tricalcium phosphate bone tissue engineering scaffolds enhance osteogenesis and angiogenesis in vivo. *Acta Biomater* 9:9137–9148
60. Bose S, Banerjee D, Robertson S, Vahabzadeh S (2018) Enhanced in vivo bone and blood vessel formation by iron oxide and silica doped 3D printed tricalcium phosphate scaffolds. *Ann Biomed Eng* 46:1241–1253
61. Nandi SK, Fielding G, Banerjee D, Bandyopadhyay A, Bose S (2018) 3D-printed beta-TCP bone tissue engineering scaffolds: effects of chemistry on in vivo biological properties in a rabbit tibia model. *J Mater Res* 33:1939–1947
62. Torres J, Tamimi F, Alkhraisat MH, Prados-Frutos JC, Rastikerdar E, Gbureck U et al (2011) Vertical bone augmentation with 3D-synthetic monetite blocks in the rabbit calvaria. *J Clin Periodontol* 38:1147–1153
63. Castillo M, Dias M, Vorndran E, Gbureck U, Fernandes P, Pires I et al (2014) Application of a 3D printed customized implant for canine cruciate ligament treatment by tibial tuberosity advancement. *Biofabrication* 6
64. Arcos D, Vallet-Regi M (2013) Bioceramics for drug delivery. *Acta Mater* 61:890–911
65. Barralet J, Gbureck U, Habibovic P, Vorndran E, Gerard C, Doillon CJ (2009) Angiogenesis in calcium phosphate scaffolds by inorganic copper ion release. *Tissue Eng Part A* 15:1601–1609
66. Uchida A, Shinto Y, Araki N, Ono K (1992) Slow release of anticancer drugs from porous calcium hydroxyapatite ceramic. *J Orthop Res* 10:440–445
67. Sudo A, Hasegawa M, Fukuda A, Uchida A (2008) Treatment of infected hip arthroplasty with antibiotic-impregnated calcium hydroxyapatite. *J Arthroplasty* 23:145–150
68. Gbureck U, Vorndran E, Muller FA, Barralet JE (2007) Low temperature direct 3D printed bioceramics and biocomposites as drug release matrices. *J Control Release* 122:173–180
69. Cornelsen M, Petersen S, Dietsch K, Rudolph A, Schmitz K, Sternberg K et al (2013) Infiltration of 3D printed tricalciumphosphate scaffolds with biodegradable polymers and biomolecules for local drug delivery. *Biomed Eng Biomedizinische Technik* 58
70. Becker ST, Bolte H, Schuenemann K, Seitz H, Bara JJ, Beck-Broichsitter BE et al (2012) Endocultivation: the influence of delayed vs. simultaneous application of BMP-2 onto individually formed hydroxyapatite matrices for heterotopic bone induction. *Int J Oral Maxillofac Surg* 41:1153–1160
71. Strobel LA, Rath SN, Maier AK, Beier JP, Arkudas A, Greil P et al (2014) Induction of bone formation in biphasic calcium phosphate scaffolds by bone morphogenetic protein-2 and primary osteoblasts. *J Tissue Eng Regen Med* 8:176–185

72. Shende P, Agrawal S (2018) Integration of 3D printing with dosage forms: a new perspective for modern healthcare. *Biomed Pharmacother* 107:146–154
73. Sandler N, Maattanen A, Ihalainen P, Kronberg L, Meierjohann A, Viitala T et al (2011) Inkjet printing of drug substances and use of porous substrates-towards individualized dosing. *J Pharm Sci* 100:3386–3395
74. Wu BM, Borland SW, Giordano RA, Cima LG, Sachs EM, Cima MJ (1996) Solid free-form fabrication of drug delivery devices. *J Control Release* 40:77–87
75. Yu DG, Yang XL, Huang WD, Liu J, Wang YG, Xu H (2007) Tablets with material gradients fabricated by three-dimensional printing. *J Pharm Sci* 96:2446–2456
76. Wu W, Zheng Q, Guo X, Sun J, Liu Y (2009) A programmed release multi-drug implant fabricated by three-dimensional printing technology for bone tuberculosis therapy. *Biomed Mater* 4
77. Fuchs A (2013) MD thesis, University of Würzburg
78. Kanter B, Geffers M, Ignatius A, Gbureck U (2014) Control of in vivo mineral bone cement degradation. *Acta Biomater* 10:3279–3287